atmosphere

MDPI

Article

Insights on In-Situ Photochemistry Associated with Ozone Reduction in Guangzhou during the COVID-19 Lockdown

Kit Ying Shek [1], Yangzong Zeren [1], Hai Guo [1], Mei Li [2,3,4], Ming Liu [5], Bo Huang [5] and Xiaopu Lyu [1,*]

[1] Department of Civil and Environmental Engineering, The Hong Kong Polytechnic University, Hong Kong 999077, China; kynicole.shek@connect.polyu.hk (K.Y.S.); yangzong.zeren@connect.polyu.hk (Y.Z.); hai.guo@polyu.edu.hk (H.G.)
[2] Institute of Mass Spectrometry and Atmospheric Environment, Jinan University, Guangzhou 510632, China; limei@jnu.edu.cn
[3] Guangdong Provincial Engineering Research Center for On-Line Source Apportionment System of Air Pollution, Guangzhou 510632, China
[4] Guangdong-Hongkong-Macau Joint Laboratory of Collaborative Innovation for Environmental Quality, Guangzhou 510045, China
[5] Guangzhou Hexin Instrument Co., Ltd., Guangzhou 510530, China; m.liu@hxmass.com (M.L.); b.huang@hxmass.com (B.H.)
* Correspondence: xiaopu.lyu@polyu.edu.hk

Abstract: Increases in ground-level ozone (O_3) have been observed during the COVID-19 lockdown in many places around the world, primarily due to the uncoordinated emission reductions of O_3 precursors. In Guangzhou, the capital of Guangdong province in South China, O_3 distinctively decreased during the lockdown. Such a phenomenon was attributed to meteorological variations and weakening of local O_3 formation, as indicated by chemical transport models. However, the emission-based modellings were not fully validated by observations, especially for volatile organic compounds (VOCs). In this study, we analyzed the changes of O_3 and its precursors, including VOCs, from the pre-lockdown (Pre-LD) to lockdown period (LD) spanning 1 week in Guangzhou. An observation-based box model was applied to understand the evolution of in-situ photochemistry. Indeed, the ambient concentrations of O_3 precursors decreased significantly in the LD. A reduction of 20.7% was identified for the total mixing ratios of VOCs, and the transportation-related species experienced the biggest declines. However, the reduction of O_3 precursors would not lead to a decrease of in-situ O_3 production if the meteorology did not change between the Pre-LD and LD periods. Sensitivity tests indicated that O_3 formation was limited by VOCs in both periods. The lower temperature and photolysis frequencies in the LD reversed the increase of O_3 that would be caused by the emission reductions otherwise. This study reiterates the fact that O_3 abatement requires coordinated control strategies, even if the emissions of O_3 precursors can be significantly reduced in the short term.

Keywords: ground-level ozone; volatile organic compounds; in-situ photochemistry; photochemical box model; COVID-19 lockdown

Citation: Shek, K.Y.; Zeren, Y.; Guo, H.; Li, M.; Liu, M.; Huang, B.; Lyu, X. Insights on In-Situ Photochemistry Associated with Ozone Reduction in Guangzhou during the COVID-19 Lockdown. *Atmosphere* **2022**, *13*, 212. https://doi.org/10.3390/atmos13020212

Academic Editor: Ilias Kavouras

Received: 6 January 2022
Accepted: 26 January 2022
Published: 28 January 2022

1. Introduction

Tropospheric ozone (O_3) is mainly produced through reactions between volatile organic compounds (VOCs) and nitrogen oxides (NO_x) in the presence of sunlight [1]. In general, O_3 production is limited by either VOCs, NO_x, or both. Reducing emissions of reactive VOCs is effective for O_3 control in a VOC-limited regime, while it is more preferable to reduce NO_x emissions in a NO_x-lean environment [2]. Therefore, identifying the formation regime is essential for O_3 control. O_3 pollution is also sensitive to meteorological conditions. Strong solar radiation, high temperature, low relative humidity, and weak winds generally lead to an aggravation of O_3 pollution [3,4].

To reduce the transmission of COVID-19, a series of social distancing and epidemic prevention actions have been implemented by many local governments since late January 2020. Table 1 summarizes the major events that happened in Guangdong province in the early stage of the COVID-19 outbreak. The first-level response to major public health emergencies was initiated 2 days after the first case was confirmed in Guangdong province on 21 January 2020. Most of the public transport was suspended between Wuhan (the city where the first known case was identified) and Guangdong. Movement restriction in residential areas and closure of schools and entertainment venues were also implemented in Guangzhou from 24 January 2020 onwards [5]. The restrictions were not relaxed until 23 February, when the first-level response was adjusted to second-level. Since then, the industries and companies in Guangzhou progressively resumed operation. In early May 2020, the response level was further lowered and the lockdown was almost lifted.

Table 1. Major events happened in Guangdong province in relation to COVID-19 during 21 January–24 February 2020.

Date	Location	Event
21 January	Guangdong Province	The first case in Guangdong province was confirmed
23 January–23 February	Guangdong Province	First-level emergency response was initiated; Lockdown was announced in Wuhan
24 January	Guangzhou	Lockdown was announced
25 January	China	Chinese New Year's Eve
10 February	Guangdong Province	Partial resumption of work
17 February	Huangpu District (Guangzhou)	Full resumption of work
24 February	Guangzhou	First-level emergency response was downgraded to second-level

As a result of the COVID-19 lockdown, emissions of a wide range of air pollutants, including O_3 precursors, were reduced [6,7]. It was indicated that the ambient concentrations of criteria air pollutants, i.e., fine particulate matters ($PM_{2.5}$), respirable suspended particulates (PM_{10}), carbon monoxide (CO), nitrogen dioxide (NO_2), and sulfur dioxide (SO_2), exhibited significant reductions in many Chinese cities [6,7]. However, the ground-level O_3 increased in most of the urban areas, the same as for some other secondary air pollutants [8]. For example, Li et al. [9] found that O_3 increased noticeably by 84.1% in the North China Plain (NCP) during the lockdown. An increment of 49.5% was observed for O_3 in southwestern China [10]. The average enhancement was determined to be 112% and 73% across 184 sites in North China and 108 sites in Central China, respectively [11]. It is interesting to note the high values of O_3 decreased in some areas of the Pearl River Delta (PRD) region during the COVID-19 lockdown, despite the increase of nighttime O_3 [12]. Emission reductions and changes in meteorological conditions were tentatively regarded as the main causes of the O_3 decrease [12–14].

However, most of the studies were grounded on emission-based models [6,12,14], and the results were subject to uncertainties of emission inventories and lacked adequate validation by observation data, especially for VOCs. Such deficiencies might impede accurate representation of the chemical processes. Qi et al. [15] and Wang et al. [16] analyzed the changes of VOCs using online measurement data and explored the O_3 formation chemistry with diagnostic ratios in Guangzhou and Nanjing during the lockdown. However, the diagnostic ratios could hardly indicate detailed in-situ photochemistry, e.g., sensitivities of O_3 formation to the precursors and meteorological parameters.

In this study, by using 1-week comprehensive observation data, we analyze the changes of O_3 and its precursors from the pre-lockdown (Pre-LD) to lockdown (LD) period at an urban site in Guangzhou. In particular, the evolutions of VOC mixing ratios and compositions are discussed. A photochemical box model constrained by observations is applied to simulate the in-situ photochemistry. The reasons for lower O_3 during the lock-

down are explored with sensitivity tests, according to which the impacts of meteorological conditions (especially temperature and solar radiation) are highlighted.

2. Methodology

2.1. Data Sources

Criteria air pollutants (O_3, NO_2, CO, SO_2, $PM_{2.5}$, and PM_{10}) and nitric oxide (NO) were continuously measured at an urban site in Guangzhou, i.e., No. 86 Secondary School (Figure 1). The site (23.10° N, 113.44° E) is located in Huangpu district, one of the fast-developing industrial districts in Guangzhou and an important area for international trade and investment. The district is home to ~20.8% of the industrial enterprises in Guangdong province, including, but not limited to, electronics manufacturing, automotive manufacturing, electricity and heat supply industry, and petrochemical industry. Surrounding the site is an urban center, where the population and number of registered vehicles are 15.3 million and 2.8 million, respectively.

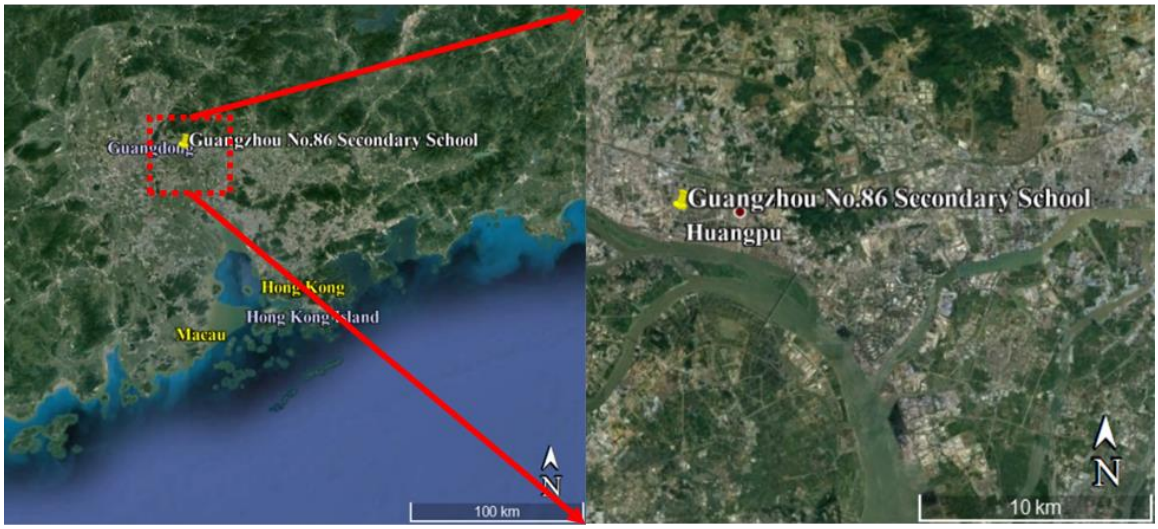

Figure 1. Location of the sampling site. The background figure is taken from Google Maps.

We adopted the data collected from 1 January to 17 February 2020, covering the Pre-LD period (1–24 January 2020) and LD period (25 January–17 February 2020). The trace gases, $PM_{2.5}$ and PM_{10}, were measured by the commercial instruments (Thermo Scientific, Waltham, MA, USA), which were regularly calibrated. Meteorological data, including wind speed, wind direction, pressure, temperature, relative humidity, and solar radiation, were monitored using an automated weather station. In addition, the photolysis frequencies of NO_2, O_3, formaldehyde (HCHO), hydrogen peroxide (H_2O_2), nitrous acid (HONO), and nitrate radical (NO_3) were measured using a charge coupled device (CCD) detector.

The valid VOC measurement was only performed during 8–27 January 2020, using an online gas chromatography coupling with mass spectrometer and flame ionization detector (Chromatotec, Saint-Antoine, France). To ensure data quality, a standard operating procedure was established and implemented. Zero air was analyzed once a week, and it was required that the background mixing ratios for all the species of interest were lower than the respective detection limits or 0.1 ppbv, whichever was lower. Single point verification with mixed standards of median concentrations was performed weekly. The allowable standard errors were <20%. The sampling flow was checked every month, and the deviations were well within ±10%. Standard curves were updated quarterly, and the correlation coefficients were higher than 0.99 for all the species of interest. In total, 103 species were measured. We focused on 45 out of 103 species with relatively good data quality and data completeness in this study.

As VOCs were measured in a much shorter period, the analyses of VOCs and photochemistry were mainly carried out in a transitional week covering four Pre-LD days

(20–23 January 2020) and three LD days (25–27 January 2020). The LD period overlapped with the Chinese New Year (CNY) (25–31 January 2020), which might also influence the emissions of some air pollutants. For example, $PM_{2.5}$, PM_{10}, and SO_2 achieved their peak values at 01:00 a.m. on CNY's eve and the concentrations fell back to the levels before the ascents within 2 h (Figure S1). Such patterns were most likely due to the temporary and intensive burning of fireworks [17,18]. Because VOCs CO and NO_x did not experience obvious enhancements on CNY's eve, and we focused on O_3 photochemistry in daytime, the data on 25 January were not excluded from the analysis.

2.2. Missing Data Treatment and Uncertainty

Due to instrument maintenance, the VOC data were not available during 08:00 a.m.–16:00 p.m. on 26 January and 14:00 p.m.–18:00 p.m. on 27 January. The missing data were estimated using a scaling method, as described in Equation (1). The method assumes that the diurnal patterns of individual VOCs on 26 and 27 January were the same as those on 25 January. To correct the differences caused by emissions and meteorology, CO was adopted as a reference species.

$$\frac{X_i/\overline{X}}{CO_i/\overline{CO}} = \frac{Y_i/\overline{Y}}{CO'_i/\overline{CO'}} \quad (1)$$

where X_i (Y_i) and CO_i (CO'_i) represent the mixing ratios of individual VOCs and CO at the ith hour on 26/27 January (25 January), respectively. $\overline{X}$ ($\overline{Y}$) and $\overline{CO}$ ($\overline{CO'}$) are the average mixing ratios of the corresponding species in the time interval of 00:00 a.m.–07:00 a.m. on 26/27 January (25 January), when the data were most complete.

It was inevitable that the estimated mixing ratios of the VOCs were subject to certain uncertainties, because the emissions and chemical transformations of the VOCs did not necessarily follow the same patterns as those for CO. The estimated mixing ratios of VOCs were only used in modelling of the in-situ photochemistry. To examine the uncertainty propagation, we performed sensitivity tests for the simulated O_3 production rate. As shown in Figure S2, 20% (−20%) changes in the estimated mixing ratios of VOCs led to variations of O_3 production rate by 23.9% (−23.7%) and 8.55% (−10.2%) on 26 and 27 January during 07:00 a.m.–16:00 p.m., respectively. We remind readers of the uncertainties associated with the missing data.

2.3. Photochemical Box Model

A photochemical box model coupled with the Master Chemical Mechanism (v3.2), termed PBM-MCM hereinafter, was used for in-situ photochemistry modelling. As a near-explicit chemical mechanism, MCM v3.2 describes ~16,500 atmospheric homogeneous reactions for ~5900 chemical species. To make it well constrained, the model read the observation data and the estimated the mixing ratios of VOCs every 200 s. It included 45 VOCs, 2 oxygenated VOCs (OVOCs), 5 trace gases, temperature, relative humidity, and photolysis frequencies for 6 species (O_3, NO_2, H_2O_2, NO_3, HCHO, and HONO), as listed in Table S1. It is noteworthy that O_3 was not constrained by observation when the model was used to simulate O_3. For the simulation on a specific day, the model ran with the same chemical and meteorological profiles for 5 days, and the simulation on the first 4 days was for spin-up. More details about the model have been introduced elsewhere [19,20].

The sensitivity of O_3 formation to the precursors and meteorological parameters is characterized using relative incremental reactivity (RIR), which is calculated following Equation (2).

$$\mathrm{RIR(X)} = \frac{\left[P^S_{O_3-NO}(X) - P^S_{O_3-NO}(X-\Delta X)\right]/P^S_{O_3-NO}(X)}{\frac{\Delta S(X)}{S(X)}} \quad (2)$$

where $S(X)$ and $\Delta S(X)$ represent the observed mixing ratios (or values) of precursor (or meteorological parameter) X and 10% reduction in the mixing ratios (or values), respectively.

$P^S_{O_3-NO}(X)$ is the net O_3 production rate simulated in the base run with observed mixing ratios of precursors and real values of meteorological parameters, while $P^S_{O_3-NO}(X-\Delta X)$ denotes the simulated O_3 production rate with a 10% reduction in mixing ratios (or values) for X. The net O_3 production rate is calculated by adding up the reaction rates of O_3 production and destruction pathways (Table S2), represented by positive and negative values, respectively. Higher absolute values of RIR indicate higher sensitivities of O_3 formation to the precursors (or meteorological parameters), with positive and negative values representing contribution and destruction of the precursor (meteorological parameter) to O_3 formation, respectively.

3. Results and Discussion

3.1. Meteorological Conditions and Trace Gases

Table 2 summarizes the statistical results of air pollutants and meteorological conditions, as well as the changes from Pre-LD to LD. The results are presented and discussed separately for a longer period and a shorter period, due to the much less VOC data as stated above.

Within the longer period (1 January–17 February), higher temperature, lower wind speed, and lower relative humidity, the meteorological conditions favorable for O_3 formation and accumulation were observed during the Pre-LD. Likewise, the meteorological conditions showed similar patterns between the Pre-LD and LD in the shorter study period. In addition, both the solar radiation (Pre-LD: 256 ± 52.2 W/m^2, LD: 164 ± 55.8 W/m^2, *p*-value: 0.03) and photolysis frequency of NO_2 (Pre-LD: 1.34 ± 0.36 × 10^{-3} s^{-1}, LD: 0.74 ± 0.33 × 10^{-3} s^{-1}, *p*-value: 0.02) were significantly lower during the LD in the shorter study period. The north winds prevailed during the LD, differing from the weak winds with varying directions during the Pre-LD. Furthermore, the reanalysis data version 5 (v5) from the European Centre for Medium-Range Weather Forecasts (ERA5) showed a large difference (*p*-value: 0.10) in boundary layer height between the two periods (average of 404 m in the Pre-LD and 569 m in the LD), indicating worse dispersion conditions in the Pre-LD. Overall, the comparisons clearly indicate that the meteorological conditions were more conducive to O_3 pollution during Pre-LD.

In the longer period, the average concentrations (or mixing ratios) of $PM_{2.5}$, PM_{10}, CO, SO_2, NO_2, and NO during the LD decreased by 33.0%, 55.9%, 18.5%, 41.7%, 60.4%, and 79.2% relative to those during Pre-LD, respectively (Table 2). The results indicate that the COVID-19 lockdown indeed made a significant contribution to air quality improvement in Guangzhou, consistent with the findings of previous studies [6,12].

Comparable reduction percentages were determined in the shorter study period, except for CO. It is surprising that the mixing ratios of CO increased by 8.28% during the LD in the shorter period. Such an increase was also observed at 38 out of 50 stations in the eight other cities in inland PRD, according to the data grabbed from the China National Environmental Monitoring Centre. An average increase of 7.96 ± 3.86% (*p*-value: 0.15) was determined for CO in the eight cities. However, CO decreased by 7.30% and 10.6% in Hong Kong and Macau in the corresponding periods, respectively. Therefore, the rises in CO levels in Guangzhou and the surrounding cities were more likely caused by emissions sharing similar patterns in the inland PRD. The correlation analysis indicates that the coefficients of determination (R^2) for the correlations between CO and some VOC species were significantly elevated during LD (Table S3). The VOCs included ethane, propane, ethene, ethyne, benzene, and 1,2-dichloroethane, which are usually regarded as tracers of combustion activities [21,22]. The time series of CO and ethyne in the shorter study period are shown in Figure S3. CO showed a pronounced increase from 06:00 a.m. to 23:00 p.m. on 25 and 26 January, together with an enhancement of ethyne. During CNY, family gathering and celebration with activities of burning incense and joss paper, cooking, barbecuing, and grilling are common [23]. These family-based activities were in compliance with the epidemic prevention regulations. Therefore, the rise in CO levels during LD might be associated with some combustion activities during CNY.

Table 2. Changes in meteorological conditions and concentrations (or mixing ratios) of air pollutants between the Pre-LD and LD periods. Blanks represent uncalculated values.

Parameter or Species	Longer Period				Shorter Period				Percentage Change				
	Pre-LD (1–24 January)		LD (25 January–17 February)		Pre-LD (20–24 January)		LD (25–27 January)		Longer Period (This Study)		Shorter Period (This Study)		Wang et al. [12]
	Mean	95% C.I. #	Mean	95% C.I.	Mean	95% C.I.	Mean	95% C.I.	Change	*p*-Value *	Change	*p*-Value	Change
Temperature (°C)	19.2	0.30	15.4	0.28	20.1	0.70	14.1	0.90	−19.5%	<0.001	−29.9%	<0.001	−20.8%
Wind speed (m/s)	1.33	0.05	1.57	0.04	1.09	0.01	2.10	0.13	18.1%	<0.001	92.3%	<0.001	
Relative humidity (%)	58.7	0.76	60.6	1.34	61.9	1.58	64.9	2.20	3.20%	0.02	4.82%	0.03	
$PM_{2.5}$ ($\mu g/m^3$)	31.5	1.29	21.1	1.13	24.3	1.62	14.9	2.91	−33.0%	<0.001	−38.8%	<0.001	−33.8%
PM_{10} ($\mu g/m^3$)	63.2	2.81	27.9	1.50	38.5	2.47	19.3	3.71	−55.9%	<0.001	−49.8%	<0.001	
CO (ppbv)	734	12.3	598	8.09	661	22.5	716	30.9	−18.5%	<0.001	8.28%	<0.01	
SO_2 (ppbv)	2.44	0.11	1.42	0.05	1.51	0.08	1.08	0.31	−41.7%	<0.001	−28.7%	<0.01	
NO_2 (ppbv)	29.4	1.29	11.7	0.66	19.5	1.51	6.36	0.49	−60.4%	<0.001	−67.4%	<0.001	−64.7%
NO (ppbv)	15.0	2.59	3.12	0.64	3.29	0.95	1.14	0.17	−79.2%	<0.001	−65.4%	<0.001	
DMA8 O_3 (ppbv)	39.2	1.20	30.3	0.99	46.8	2.20	24.7	1.94	−22.8%	<0.01	−47.2%	<0.001	−21.3%
TVOC (ppbv)					46.9	3.29	37.1	2.02			−20.7%	<0.001	
Alkanes (ppbv)					20.3	1.66	15.1	0.85			−25.4%	<0.001	
Alkenes (ppbv)					3.85	0.53	2.44	0.23			−35.1%	<0.001	
Alkyne (ppbv)					6.45	0.37	7.86	0.76			21.9%	<0.001	
Aromatics (ppbv)					8.51	0.57	6.70	0.31			−21.2%	<0.001	
Halocarbons (ppbv)					2.78	0.31	2.44	0.18			−11.0%	0.13	
OVOCs (ppbv)					5.04	0.85	2.51	0.39			−50.1%	<0.001	

95% confidence interval; * *p*-Value is calculated from two-tailed *t*-test.

The daily maximum 8-hour average (DMA8) O_3 decreased by 22.8% and 47.2% from the Pre-LD to LD in the longer and shorter study period, respectively (Table 2). This O_3 reduction was opposite to the widely reported O_3 increases in many other regions of China and the world during the COVID-19 lockdown [6,24]. In fact, the nocturnal O_3 did increase during LD (Figure S4), which could be explained by the weakening of NO titration. However, the reduction of DMA8 O_3 indicated that weakening of NO titration that has been regarded as the main cause of O_3 increase during COVID-19 lockdown did not dominate over the other factors modulating the changes of O_3 in Guangzhou. The underlying reasons merit an in-depth analysis from chemical and meteorological perspectives.

3.2. Changes in Mixing Ratios and Compositions of VOCs

Due to the COVID-19 lockdown, the emissions of many air pollutants, including VOCs, were greatly reduced. The reduction percentages were 56.2% and 57.4% at two urban sites and 66.2% at an industrial site in Dongguan [15], 38.3% at an urban site and 50.3% at a rural site in Shanghai [25], 46.0% at a mix of suburban and industrial site in Nanjing [16], and 65.2% at a suburban site in Tianjin [26]. According to Huang et al. [8], VOC emissions in Guangdong province experienced a reduction of 46% during LD. In this study, the sum of 27 alkanes, 10 alkenes, 1 alkyne, 21 aromatics, 29 halocarbons, and 15 OVOCs species, termed as TVOCs, exhibited a decline in total mixing ratios of 9.71 ppbv (20.7%) during LD in the shorter study period (Table 2). Moreover, the levels of TVOCs were more stable in LD, as indicated by the lower coefficient of variation, i.e., 0.31 in Pre-LD and 0.19 in LD. This also implied the less intensive emissions (e.g., vehicle emissions in rush hours) during the lockdown. However, it is obvious that the reduction of VOCs in Guangzhou was less significant than in many other cities. As discussed above, the emissions of a few VOC species might have been enhanced due to family-based activities during the CNY. The effect was more significant in this study because of the shorter study period. Underestimating the reduction of VOCs would influence the assessment of the effects of COVID-19 lockdown on in-situ O_3 production, which is illustrated in Section 3.3.

Alkanes, alkenes, aromatics, halocarbons, and OVOCs decreased by 25.4%, 35.1%, 21.2%, 11.0%, and 50.1% during LD, respectively (Table 2). The largest reductions of alkenes and OVOCs were most likely attributed to the transportation sector, because alkenes in urban air are mainly from vehicle emissions [27], and methyl *tert*-butyl ether (MTBE), a typical tracer of vehicle emissions [28,29], was the OVOC species that experienced the biggest drop in mixing ratios (see discussions below). The lowest and insignificant (p-value: 0.13) reduction of halocarbons might suggest some industries were still in operation in LD. Ethyne, the only alkyne that was detected, had mixing ratios 21.9% higher during the LD than during the Pre-LD. As a result of the inconsistent changes, the fractions of these groups of VOCs in TVOCs also changed slightly (Figure 2). Most notably, OVOCs accounted for 6.77 $\pm$ 1.05% of the TVOCs during LD, ~4% lower than that during Pre-LD. Conversely, the fraction of alkyne in TVOCs increased from 13.8 $\pm$ 0.80% during Pre-LD to 21.2 $\pm$ 2.06% during LD.

Furthermore, we looked into the changes of individual VOC species from Pre-LD to LD. As shown in Figure 3, the mixing ratios for most of the alkanes decreased during LD, and the reduction percentage ranged from 1.90 % for ethane to 55.2% for *i*-butane. The notable reduction of *i*-butane, a typical tracer of liquefied petroleum gas (LPG) in Guangzhou [30,31], indicated a significant drop in the activity level of LPG-powered vehicles (e.g., taxis and public buses) during LD. In fact, reductions were also observed for propane (34.9%) and *n*-butane (45.7%), which are also the main components of LPG. As for alkenes, propene, *trans*-2-butene and 1-pentene had much lower mixing ratios during LD, which seemed to be the result of the restrained vehicular emissions [32,33]. Among aromatics, toluene, ethylbenzene, and *m*,*p*-xylenes were the species that experienced the most significant reductions. According to the established knowledge on their sources in Guangzhou [21,34], the decreases were most likely due to reduced emissions from transportation and industries.

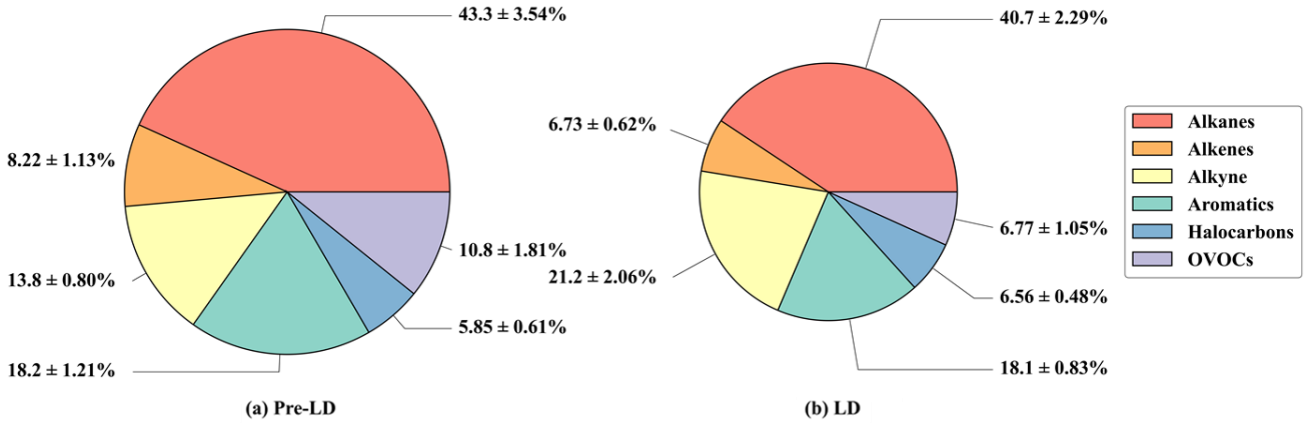

Figure 2. VOC compositions during the (**a**) Pre-LD and (**b**) LD in the shorter study period. Pie area is proportional to the mixing ratio of TVOCs.

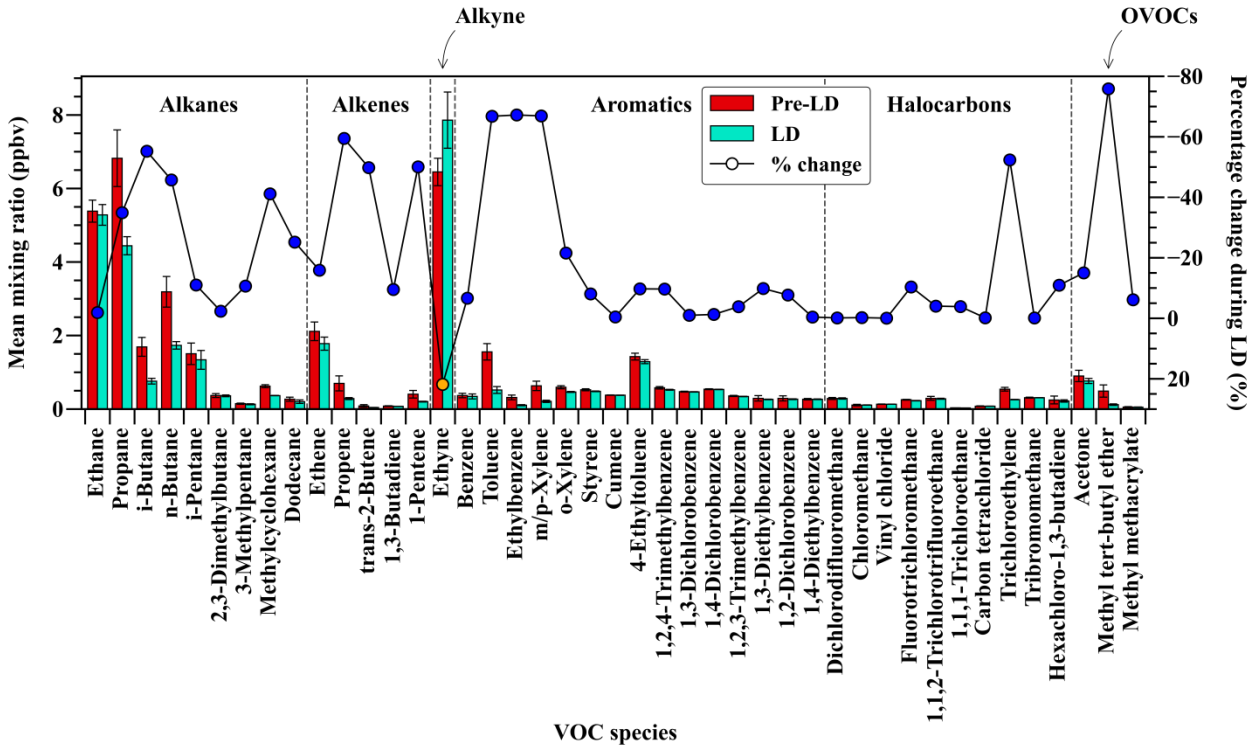

Figure 3. Average mixing ratios of individual VOCs during Pre-LD (red bar) and LD (green bar), and their percentage changes (blue circle: reduction; orange circle: increase). Error bars represent 95% confidence intervals. The changes and *p*-values are listed in Table S4.

Fluorotrichloromethane (CFC-11) and trichloroethylene, two halocarbons, decreased by 10.4% and 52.3% during LD, respectively. It is not surprising to note the reduction of trichloroethylene, because of the halting of dry-cleaning services and many industrial activities, e.g., electronics manufacturing, where trichloroethylene is used as degreaser [35]. However, the higher levels of CFC-11 during Pre-LD might imply that some sources of CFC-11 still existed in Guangdong province, even though its use has been officially banned in China. As a typical tracer of vehicle emissions [28,29], MTBE was observed with noticeably lower mixing ratios during LD. Overall, the changes for most of the VOCs could be explained by the reductions of vehicular and industrial emissions during the COVID-19 lockdown. The increase in mixing ratios of ethyne, most likely relating to some combustion activities during CNY, has been explained before.

3.3. In-Situ O_3 Formation and Sensitivities

First, we ran the PBM-MCM model to simulate O_3 where O_3 was not constrained by observation. Figure S5 compares the simulated and observed O_3 during 07:00 a.m.–16:00 p.m. from 20 to 27 January, excluding 24 January when there was no VOC data. Overall, the variations and magnitudes of the observed O_3 were reasonably simulated. The index of agreement, calculated following the equation in [36], was 0.82, which was acceptable for the performance of a box model [19,37]. It is unreasonable to expect a box model to exactly reproduce observations, because of the insufficient or even complete lack of representation of physical processes.

In order to better simulate the in-situ photochemical processes, we then ran the model under O_3 constraints. Figure 4 shows the variations of the simulated net O_3 production rate and the observed O_3. Consistent with the pattern of observed O_3 between Pre-LD and LD, the daytime (07:00 a.m.–16:00 p.m.) average net O_3 production rate in Pre-LD (0.96 ± 0.20 ppbv/h) was significantly (p-value: 0.05) higher than that in LD (0.70 ± 0.16 ppbv/h). The DMA8 net O_3 production rate also decreased from 1.1 ± 0.53 ppbv/h in Pre-LD to 0.82 ± 0.22 ppbv/h in LD. However, the reduction percentage (25.5%) was much lower than that for the observed DMA8 O_3 (47.2%, Table 2). Therefore, in addition to the weaker photochemical formation locally, physical processes, such as regional transport, also contributed to the reduction of O_3 in LD.

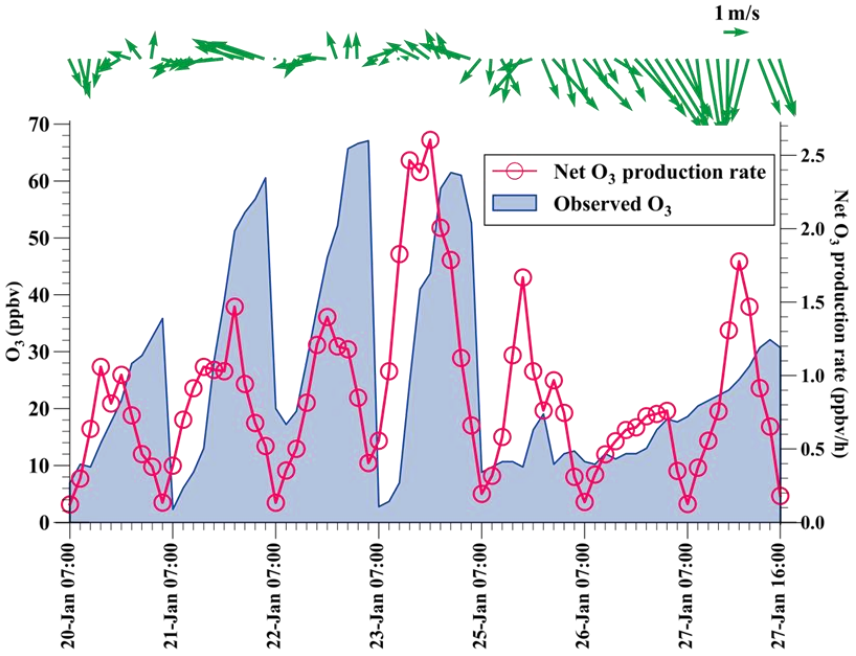

Figure 4. Variations of the net O_3 production rate and observed O_3 during 07:00 a.m.–16:00 p.m. from 20 to 27 January, excluding 24 January. Green arrows denote wind fields.

It should be noted that the in-situ O_3 formation was related to not only emissions but also to meteorology. Namely, the lower in-situ O_3 production in LD did not necessarily mean the emission reductions during COVID-19 lockdown were effective in reducing local O_3 formation. Hence, we examined the effects of meteorology on in-situ O_3 formation through swapping meteorological conditions (temperature, relative humidity, and photolysis frequencies) between the simulations in Pre-LD and LD. For convenience, the base simulations were constructed and constrained by the average diurnal profiles of air pollutants and meteorology in Pre-LD and LD, respectively. Figure 5 presents the average diurnal variations of the simulated net O_3 production rate in the Pre-LD and LD periods. The simplified simulation overestimated the net O_3 production rate, especially in the Pre-LD period. However, the pattern between the two periods (i.e., lower net O_3 production rate in the LD) was well simulated.

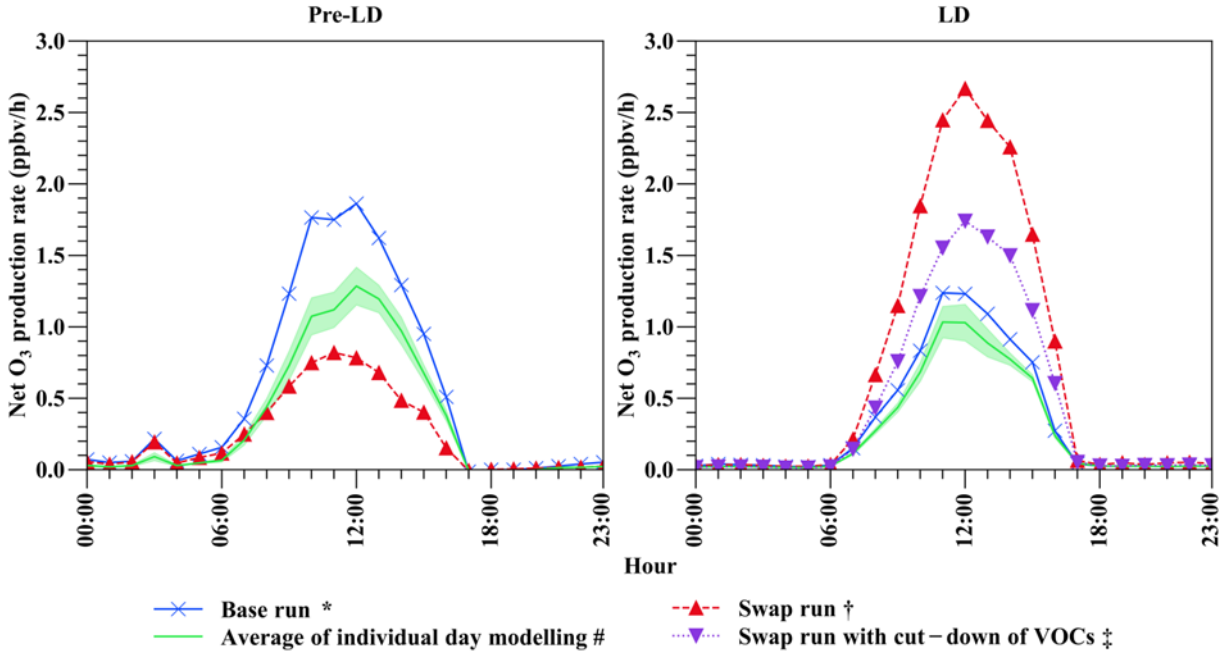

Figure 5. Average diurnal variations of the net O_3 production rate during Pre-LD and LD. * Base runs with the average profiles and no swap. # Averages of the modelling results on individual days in Pre-LD and LD, respectively (no swap). † Simulations with swap of the averaged diurnal profiles of meteorology between Pre-LD and LD. ‡ Simulation with Pre-LD meteorology and LD chemical profiles with a further cut-down of VOCs by 31.6%. Shaded area on the green line denotes the 95% confidence interval.

After the meteorological conditions were swapped, the daytime (07:00 a.m.–16:00 p.m.) net O_3 production rate in Pre-LD decreased significantly from 1.21 ± 0.34 ppbv/h to 0.53 ± 0.14 ppbv/h by −56.1%. In contrast, it increased by 119% in LD. With the same meteorological profiles, the O_3 production rates in LD were much higher than those in Pre-LD. The results suggest that meteorological conditions played critical roles leading to O_3 reduction in the LD. It is inferred that some additional emissions during CNY might elevate the levels of certain VOCs in LD. To account for the interference, O_3 production was simulated in another assumed scenario where the VOCs were further reduced by 31.6% on top of the swap run in the LD. This scenario assumes the mixing ratios of VOCs decreased by 46% in the LD relative to those in Pre-LD, in line with the reduction percentage in Guangdong province based on the emission inventories [8]. As shown in Figure 5, the daytime (07:00 a.m.–16:00 p.m.) net O_3 production rates (1.07 ± 0.34 ppbv/h) decreased relative to those in the swap run of LD (1.62 ± 0.53 ppbv/h), but they turned out to be comparable (p-value: 0.58) to the rates in Pre-LD (1.21 ± 0.34 ppbv/h). Therefore, even if the VOCs were reduced by 46%, the in-situ O_3 production rate would not decrease in LD if the meteorology did not change. This provides a semi-quantitative assessment on how the meteorology led to the difference in O_3 levels between the Pre-LD and LD periods.

To further understand the effects of meteorology on O_3 formation, the sensitivities of the net O_3 production rate to O_3 precursors and meteorological parameters were tested. Figure 6 shows the average RIR values of the air pollutants or the parameters in the two periods. The negative RIR of NO_x indicated that O_3 formation was limited by VOCs, especially in the Pre-LD period. Due to the substantial reduction of NOx mixing ratios, the absolute value of RIR for NO_x decreased from 0.86 ± 0.08 in Pre-LD to 0.19 ± 0.06 in LD. The net O_3 production rate responded positively and most sensitively to anthropogenic VOCs (AVOCs), which was followed by photolysis frequencies and temperature in both periods. The sensitivities to CO and relative humidity were relatively low. The RIR of AVOCs during LD (1.16 ± 0.02) was lower than that in Pre-LD (1.44 ± 0.03), likely resulting

from the reduction of VOCs. While the RIR of photolysis frequencies was experienced also from 1.08 ± 0.09 to 0.95 ± 0.08, a more significant decrease was identified for the RIR of temperature, i.e., 0.92 ± 0.12 in Pre-LD and 0.46 ± 0.06 in LD.

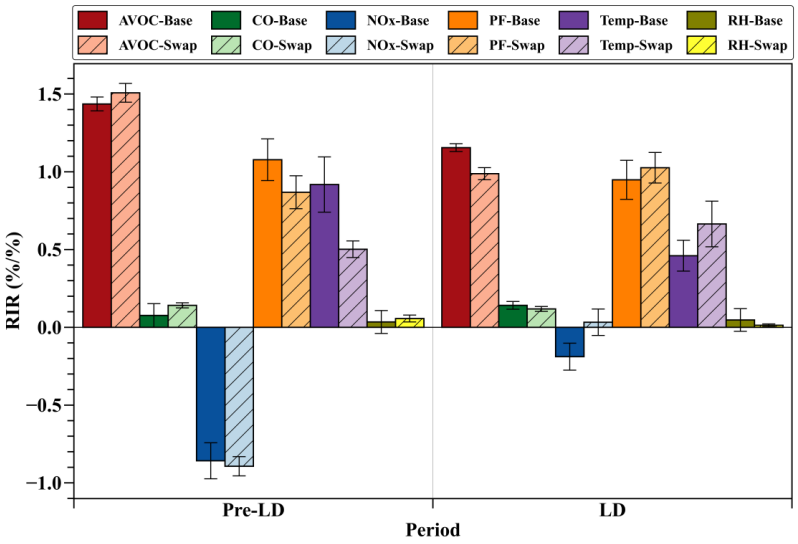

Figure 6. Average RIR values of anthropogenic VOCs (AVOC), CO, NO_x, photolysis frequencies (PF), temperature (Temp), and relative humidity (RH) determined in the base runs (Base) and swap runs (Swap) in two periods. Error bars represent the 95% confidence intervals.

In the swap runs where the observed values of meteorological parameters in the Pre-LD and LD were swapped, the most obvious change was that the RIR of NO_x became positive, albeit small, in LD (0.03 ± 0.06). Namely, O_3 formation in LD would be in a transitional regime otherwise, if the meteorology did not change between Pre-LD and LD. This partially explained why the net O_3 production rate increased so much in the swap run during LD (Figure 5), because O_3 formation was most efficient in the transitional regime. Correspondingly, the RIR of AVOCs decreased, which was a normal change from a VOC-limited regime to a transitional regime. In addition, the swap of meteorology also resulted in higher RIR values of photolysis frequencies and temperature in LD. Conversely, the sensitivities of O_3 formation to both parameters decreased markedly in Pre-LD if the meteorology was placed with that in LD.

Overall, the decrease of in-situ O_3 production in the LD was mainly caused by meteorological changes, which also had an impact on O_3 formation sensitivity. To our knowledge, this is the first time the roles of meteorology in lowering the in-situ O_3 production rate in South China have been semi-quantitatively characterized based on observation data. However, it should be kept in mind that the chemical profiles that drove the model were also influenced by meteorological conditions. The effects are not decoupled in this study.

4. Conclusions

The COVID-19 lockdown has had a profound impact on air quality all over the world, which also provides a rare opportunity to look into the atmospheric chemistry under the scenario of substantially reduced anthropogenic emissions. Furthermore, the current air pollution control strategies can be examined, and more effective solutions to some tough problems, e.g., tropospheric O_3 pollution, may be proposed. In the first quarter of 2020, a lockdown was imposed across most Chinese cities due to the raging epidemic. While the emissions of a majority of air pollutants were reduced drastically, ground-level O_3 was found to be increased in many cities. An exception was Guangzhou, a megacity in South China, where the urban O_3 even decreased during the COVID-19 lockdown. A key question hidden behind this phenomenon was whether the emission reduction was effective for O_3 control in South China or at least this city. Emission-based modelling

studies gave a somewhat affirmative answer, although O_3 reduction was also attributed to meteorological effects. Based on the observation data, we confirmed the reductions of O_3 and its precursors (both NO_x and VOCs, especially the transportation-related species) during the lockdown. Meanwhile, the changes in meteorology between the pre-lockdown and lockdown periods were also obvious. The in-situ photochemistry was revealed by an observation-based box model. According to the sensitivity tests, our answer to the above question is relatively certain: It was changes in meteorology rather than emission reduction that led to the decrease of O_3 in Guangzhou during the lockdown. In fact, if the meteorological conditions did not change, the local O_3 production would increase with the reduced emissions. Therefore, we conclude that the O_3 reduction in Guangzhou during the COVID-19 lockdown was not a successful story of human intervention in O_3 control. More coordinated schemes of emission reduction are required for the improvement of O_3 air quality.

Supplementary Materials: The following supporting information can be downloaded at: https://www.mdpi.com/article/10.3390/atmos13020212/s1, Figure S1: Variations of criteria air pollutants and NO from 12:00 on 24 January to 12:00 on 25 January; Figure S2: Responses of the simulated O_3 production rate to ±20% changes in the estimated mixing ratios of VOCs on 26 and 27 January 2020; Figure S3: Time series of CO and ethyne in the shorter study period (transitional week). The dashed line separates the Pre-LD and LD periods; Figure S4: Average diurnal profiles of O_3 during the Pre-LD and LD in the longer (left panel) and shorter study period (right panel); Figure S5: Time series of the simulated and observed O_3 between 7:00 and 16:00 on 20–27 January excluding 24 January; Table S1: VOCs, OVOCs and trace gases that are input into the PBM-MCM model; Table S2: O_3 production and destruction pathways included in calculation of net O_3 production rate; Table S3: Coefficients of determination for the correlations between CO and some VOC species during the Pre-LD and LD in the shorter study period; Table S4: Percentage changes of VOCs between the Pre-LD and LD periods and the *p*-Values.

Author Contributions: Conceptualization, X.L.; Data curation, M.L. (Mei Li), M.L. (Ming Liu) and B.H.; Formal analysis, K.Y.S.; Funding acquisition, H.G. and X.L.; Investigation, K.Y.S. and M.L. (Mei Li); Methodology, H.G. and X.L.; Resources, H.G.; Software, Y.Z.; Supervision, H.G. and X.L.; Validation, X.L.; Visualization, K.Y.S. and Y.Z.; Writing—original draft, K.Y.S.; Writing—review & editing, X.L. All authors have read and agreed to the published version of the manuscript.

Funding: This research was funded by Strategic Focus Area scheme of The Research Institute for Sustainable Urban Development at The Hong Kong Polytechnic University, 1-BBW9; Hong Kong Research Grants Council, PolyU 15219621; The Hong Kong Polytechnic University Start-up Fund for RAPs under the Strategic Hiring Scheme, 1-BD87; the Key-Area Research and Development Program of Guangdong Province, 2020B1111360001.

Institutional Review Board Statement: Not applicable.

Informed Consent Statement: Not applicable.

Data Availability Statement: The observation and modelling data are available from the corresponding author upon reasonable request.

Acknowledgments: The authors acknowledge all funders.

Conflicts of Interest: The authors declare no conflict of interest. The funders had no role in the design of the study; in the collection, analyses, or interpretation of data; in the writing of the manuscript, or in the decision to publish the results.

References

1. Atkinson, R. Atmospheric chemistry of VOCs and NO_x. *Atmos. Environ.* **2000**, *34*, 2063–2101. [CrossRef]
2. Finlayson-Pitts, B.J.; Pitts, J.N. Atmospheric Chemistry of Tropospheric Ozone Formation: Scientific and Regulatory Implications. *Air Waste* **1993**, *43*, 1091–1100. [CrossRef]
3. Jacob, D.J.; Winner, D.A. Effect of climate change on air quality. *Atmos. Environ.* **2009**, *43*, 51–63. [CrossRef]
4. Wang, T.; Xue, L.K.; Brimblecombe, P.; Lam, Y.F.; Li, L.; Zhang, L. Ozone pollution in China: A review of concentrations, meteorological influences, chemical precursors, and effects. *Sci. Total Environ.* **2017**, *575*, 1582–1596. [CrossRef]

5. Xu, T.L.; Ao, M.Y.; Zhou, X.; Zhu, W.F.; Nie, H.Y.; Fang, J.H.; Sun, X.; Zheng, B.; Chen, X.F. China's practice to prevent and control COVID-19 in the context of large population movement. *Infect. Dis. Poverty* **2020**, *9*, 115. [CrossRef]
6. Le, T.; Wang, Y.; Liu, L.; Yang, J.; Yung, Y.L.; Li, G.; Seinfeld, J.H. Unexpected air pollution with marked emission reductions during the COVID-19 outbreak in China. *Science* **2020**, *369*, 702–706. [CrossRef]
7. Silver, B.; He, X.; Arnold, S.R.; Spracklen, D.V. The impact of COVID-19 control measures on air quality in China. *Environ. Res. Lett.* **2020**, *15*, 084021. [CrossRef]
8. Huang, X.; Ding, A.; Gao, J.; Zheng, B.; Zhou, D.; Qi, X.; Tang, R.; Wang, J.; Ren, C.; Nie, W.; et al. Enhanced secondary pollution offset reduction of primary emissions during COVID-19 lockdown in China. *Natl. Sci. Rev.* **2021**, *8*, nwaa137. [CrossRef] [PubMed]
9. Li, M.; Wang, T.; Xie, M.; Li, S.; Zhuang, B.; Fu, Q.; Zhao, M.; Wu, H.; Liu, J.; Saikawa, E.; et al. Drivers for the poor air quality conditions in North China Plain during the COVID-19 outbreak. *Atmos. Environ.* **2021**, *246*, 118103. [CrossRef] [PubMed]
10. Chen, Y.; Zhang, S.; Peng, C.; Shi, G.; Tian, M.; Huang, R.J.; Guo, D.; Wang, H.; Yao, X.; Yang, F. Impact of the COVID-19 pandemic and control measures on air quality and aerosol light absorption in Southwestern China. *Sci. Total Environ.* **2020**, *749*, 141419. [CrossRef]
11. Liu, Y.; Wang, T.; Stavrakou, T.; Elguindi, N.; Doumbia, T.; Granier, C.; Bouarar, I.; Gaubert, B.; Brasseur, G. Diverse response of surface ozone to COVID-19 lockdown in China. *Sci. Total Environ.* **2020**, *789*, 147739. [CrossRef] [PubMed]
12. Wang, N.; Xu, J.; Pei, C.; Tang, R.; Zhou, D.; Chen, Y.; Li, M.; Deng, X.; Deng, T.; Huang, X.; et al. Air Quality During COVID-19 Lockdown in the Yangtze River Delta and the Pearl River Delta: Two Different Responsive Mechanisms to Emission Reductions in China. *Environ. Sci. Technol.* **2021**, *55*, 5721–5730. [CrossRef] [PubMed]
13. Li, J.; Yang, H.; Zha, S.; Yu, N.; Liu, X.; Sun, R. Effects of COVID-19 Emergency Response Levels on Air Quality in the Guangdong-Hong Kong-Macao Greater Bay Area, China. *Aerosol Air Qual. Res.* **2021**, *21*, 200416. [CrossRef]
14. Wang, S.; Zhang, Y.; Ma, J.; Zhu, S.; Shen, J.; Wang, P.; Zhang, H. Responses of decline in air pollution and recovery associated with COVID-19 lockdown in the Pearl River Delta. *Sci. Total Environ.* **2021**, *756*, 143868. [CrossRef]
15. Qi, J.; Mo, Z.; Yuan, B.; Huang, S.; Huangfu, Y.; Wang, Z.; Li, X.; Yang, S.; Wang, W.; Zhao, Y.; et al. An observation approach in evaluation of ozone production to precursor changes during the COVID-19 lockdown. *Atmos. Environ.* **2021**, *262*, 118618. [CrossRef]
16. Wang, M.; Lu, S.; Shao, M.; Zeng, L.; Zheng, J.; Xie, F.; Lin, H.; Hu, K.; Lu, X. Impact of COVID-19 lockdown on ambient levels and sources of volatile organic compounds (VOCs) in Nanjing, China. *Sci. Total Environ.* **2021**, *757*, 143823. [CrossRef]
17. Attri, A.K.; Kumar, U.; Jain, V.K. Formation of ozone by fireworks. *Nature* **2001**, *411*, 1015. [CrossRef]
18. Li, K.; Li, J.; Tong, S.; Wang, W.; Huang, R.-J.; Ge, M. Characteristics of wintertime VOCs in suburban and urban Beijing: Concentrations, emission ratios, and festival effects. *Atmos. Chem. Phys.* **2019**, *19*, 8021–8036. [CrossRef]
19. Wang, Y.; Guo, H.; Zou, S.; Lyu, X.; Ling, Z.; Cheng, H.; Zeren, Y. Surface O_3 photochemistry over the South China Sea: Application of a near-explicit chemical mechanism box model. *Environ. Pollut.* **2018**, *234*, 155–166. [CrossRef]
20. Lyu, X.; Wang, N.; Guo, H.; Xue, L.; Jiang, F.; Zeren, Y.; Cheng, H.; Cai, Z.; Han, L.; Zhou, Y. Causes of a continuous summertime O_3 pollution event in Jinan, a central city in the North China Plain. *Atmos. Chem. Phys.* **2019**, *19*, 3025–3042. [CrossRef]
21. Liu, Y.; Shao, M.; Lu, S.; Chang, C.-C.; Wang, J.-L.; Chen, G. Volatile Organic Compound (VOC) measurements in the Pearl River Delta (PRD) region, China. *Atmos. Chem. Phys.* **2008**, *8*, 1531–1545. [CrossRef]
22. Wu, F.K.; Yu, Y.; Sun, J.; Zhang, J.K.; Wang, J.; Tang, G.Q.; Wang, Y.S. Characteristics, source apportionment and reactivity of ambient volatile organic compounds at Dinghu Mountain in Guangdong Province, China. *Sci. Total Environ.* **2016**, *548–549*, 347–359. [CrossRef] [PubMed]
23. Chen, P.Y.; Tan, P.H.; Chou, C.C.K.; Lin, Y.S.; Chen, W.N.; Shiu, C.J. Impacts of holiday characteristics and number of vacation days on "holiday effect" in Taipei: Implications on ozone control strategies. *Atmos. Environ.* **2019**, *202*, 357–369. [CrossRef]
24. Tang, R.; Huang, X.; Zhou, D.; Wang, H.; Xu, J.; Ding, A. Global air quality change during the COVID-19 pandemic: Regionally different ozone pollution responses COVID-19. *Atmos. Ocean. Sci. Lett.* **2021**, *14*, 100015. [CrossRef]
25. Jia, H.; Huo, J.; Fu, Q.; Duan, Y.; Lin, Y.; Jin, X.; Hu, X.; Cheng, J. Insights into chemical composition, abatement mechanisms and regional transport of atmospheric pollutants in the Yangtze River Delta region, China during the COVID-19 outbreak control period. *Environ. Pollut.* **2020**, *267*, 115612. [CrossRef]
26. Gu, Y.; Liu, B.; Dai, Q.; Zhang, Y.; Zhou, M.; Feng, Y.; Hopke, P.K. Multiply improved positive matrix factorization for source apportionment of volatile organic compounds during the COVID-19 shutdown in Tianjin, China. *Environ. Int.* **2021**, *158*, 106979. [CrossRef]
27. Liu, Y.; Shao, M.; Fu, L.; Lu, S.; Zeng, L.; Tang, D. Source profiles of volatile organic compounds (VOCs) measured in China: Part I. *Atmos. Environ.* **2008**, *42*, 6247–6260. [CrossRef]
28. Zhang, Y.; Wang, X.; Zhang, Z.; Lü, S.; Shao, M.; Lee, F.S.C.; Yu, J. Species profiles and normalized reactivity of volatile organic compounds from gasoline evaporation in China. *Atmos. Environ.* **2013**, *79*, 110–118. [CrossRef]
29. Chang, C.C.; Lo, S.J.; Lo, J.G.; Wang, J.L. Analysis of methyl tert-butyl ether in the atmosphere and implications as an exclusive indicator of automobile exhaust. *Atmos. Environ.* **2003**, *37*, 4747–4755. [CrossRef]
30. Liu, Y.; Shao, M.; Lu, S.; Chang, C.-C.; Wang, J.-L.; Fu, L. Source apportionment of ambient volatile organic compounds in the Pearl River Delta, China: Part II. *Atmos. Environ.* **2008**, *42*, 6261–6274. [CrossRef]

31. Guo, H.; Cheng, H.R.; Ling, Z.H.; Louie, P.K.; Ayoko, G.A. Which emission sources are responsible for the volatile organic compounds in the atmosphere of Pearl River Delta? *J. Hazard. Mater.* **2011**, *188*, 116–124. [CrossRef] [PubMed]
32. Li, L.; Xie, S.; Zeng, L.; Wu, R.; Li, J. Characteristics of volatile organic compounds and their role in ground-level ozone formation in the Beijing-Tianjin-Hebei region, China. *Atmos. Environ.* **2015**, *113*, 247–254. [CrossRef]
33. Hui, L.R.; Liu, X.G.; Tan, Q.W.; Feng, M.; An, J.L.; Qu, Y.; Zhang, Y.H.; Jiang, M.Q. Characteristics, source apportionment and contribution of VOCs to ozone formation in Wuhan, Central China. *Atmos. Environ.* **2018**, *192*, 55–71. [CrossRef]
34. Guo, H.; Ling, Z.H.; Cheung, K.; Jiang, F.; Wang, D.W.; Simpson, I.J.; Barletta, B.; Meinardi, S.; Wang, T.J.; Wang, X.M.; et al. Characterization of photochemical pollution at different elevations in mountainous areas in Hong Kong. *Atmos. Chem. Phys.* **2013**, *13*, 3881–3898. [CrossRef]
35. Lyu, X.; Guo, H.; Wang, Y.; Zhang, F.; Nie, K.; Dang, J.; Liang, Z.; Dong, S.; Zeren, Y.; Zhou, B.; et al. Hazardous volatile organic compounds in ambient air of China. *Chemosphere* **2020**, *246*, 125731. [CrossRef] [PubMed]
36. Willmott, C.J. Some Comments on the Evaluation of Model Performance. *Bull. Am. Meteorol. Soc.* **1982**, *63*, 1309–1313. [CrossRef]
37. Lyu, X.; Chen, N.; Guo, H.; Zhang, W.; Wang, N.; Wang, Y.; Liu, M. Ambient volatile organic compounds and their effect on ozone production in Wuhan, central China. *Sci. Total Environ.* **2016**, *541*, 200–209. [CrossRef]